The Physics of Electron Beam Ion Traps and Advanced Research Light Sources 2005 IOP Publishing
Journal of Physics: Conference Series **72** (2007) 012011 doi:10.1088/1742-6596/72/1/012011

Theoretical studies of hyperfine effects

Per Jönsson
Malmö University, 205 06 Malmö, Sweden

Abstract. The development of space-based observatories has highlighted the need for atomic data. In this review we examine multiconfiguration methods for calculating these data. Particular emphasize is placed on hyperfine structure splittings and hyperfine induced transitions.

1. Introduction

The launch of the Hubble Space Telescope (HST) in 1990 gave a new impetus to the determination and study of isotope shifts and hyperfine structures. The importance of these parameters in astrophysics has been reviewed by Kurucz [1] and Hühnermann [2]. The high resolution of the stellar spectra obtained with the Goddard High Resolution Spectrograph aboard the HST reveals isotope shifts (IS) and hyperfine structure (hfs) of many spectral lines. In many cases, however, the small structures are not completely resolved and instead they shift and broaden the lines. To correctly interpret high resolution stellar spectra it is thus necessary to include IS and hfs in the theoretical modeling of the line profiles. The hyperfine and isotope data are needed, for instance, for calculating accurate synthetic spectra to study isotope anomalies in astronomical objects [3]. Despite numerous laboratory measurements, isotope and hyperfine data are missing for many lines, and the modeling of the line profiles has to rely on calculated values. It is therefore important to develop reliable computational methods for these parameters, as well as other broadening parameters such as Zeeman splittings, that can support the analysis.

In addition to energies and energy shifts there is an ever increasing demand for accurate radiative transition data in astrophysics [4] and in plasma and fusion research. Of special importance are weak lines that are suitable for diagnostics of electron densities in thin plasmas. For weak transitions important data with high accuracy are now produced using storage rings and EBIT light sources [5]. Experimental work is however very expensive and it is reasonable to believe that the bulk of the transition data needs to be calculated.

To meet the demand for atomic data the ATSP2K–MCHF [6], GRASP [7] and graspVU [8] computational packages have been developed and adapted to parallel computing. These packages rely on multiconfiguration methods and they contain modules for computing transition rates [9], hyperfine structures [10, 11] and isotope shifts [12], Landé factors and Zeeman splittings in intermediate fields [13]. In this paper we discuss applications of the MCHF and graspVU codes to hyperfine structure and hyperfine quenching.

2. Multiconfiguration methods

The state of a many-electron system is described by a wave function Ψ that is the solution to the wave equation

$$(\mathcal{H} - E)\Psi = 0, \tag{1}$$

where $\mathcal{H}$ is the Hamiltonian operator for the system and E the total energy. The operator $\mathcal{H}$ depends on the system as well as the underlying quantum mechanical formalism.

Light atoms are often described in the non-relativistic formalism. Here the starting point is the Hamiltonian

$$\mathcal{H} = \sum_{i=1}^{N} \left[-\frac{1}{2}\nabla_i^2 - \frac{Z}{r_i} \right] + \sum_{i<j}^{N} \frac{1}{r_{ij}}. \tag{2}$$

In the multiconfiguration Hartree-Fock (MCHF) method the wave function for a state labeled $\gamma L M_L S M_S$, where γ represents the configuration and any other quantum numbers required to specify the state, is expanded in terms of configuration state functions (CSF's) with the same parity and angular symmetry,

$$|\Psi(\gamma L M_L S M_S)\rangle = \sum_{j=1}^{M} c_j |\Phi(\gamma_j L M_L S M_S)\rangle. \tag{3}$$

The CSFs are symmetry adapted linear combinations of Slater-determinants built from a set of one-electron spin-orbitals

$$\phi_{nlm_l m_s} = \frac{1}{r} P_{nl}(r) Y_{lm_l}(\theta, \varphi) \xi_{m_s}(\sigma), \tag{4}$$

whose radial functions $\{P_{nl}\}$ need to be determined. By demanding that the energy functional should be stationary with respect to infinitesimal variations in the radial functions and expansion coefficients, a system of coupled non-linear differential equations for the radial functions is obtained along with an eigenvalue problem for the coefficients. This problem is solved iteratively by the self-consistent field method [14]. Once a set of radial functions $\{P_{nl}(r)\}$ has been obtained, a Breit-Pauli configuration interaction (CI) calculation can be performed where the wave function is expanded in LSJ coupled configuration state functions

$$|\Psi(\gamma L S J M_J)\rangle = \sum_{j=1}^{M} c_j |\Phi(\gamma_j L_j S_j J M_J)\rangle. \tag{5}$$

Now only the expansion coefficients are determined. This is done by solving the eigenvalue problem derived from the Breit-Pauli Hamiltonian which includes the most important, lowest-order corrections of the Dirac-Coulomb-Breit operator [14]. This is the intermediate coupling or LSJ approximation.

The multiconfiguration Dirac-Hartree-Fock method (MCDHF), as implemented in the GRASP and graspVU packages, is the fully relativistic counterpart to the non-relativistic MCHF scheme. In this method the Hamiltonian is given by

$$\sum_{i=1}^{N} \left[c\boldsymbol{\alpha}_i \cdot \mathbf{p}_i + (\beta_i - 1)c^2 + V_i \right] + \sum_{i<j}^{N} \frac{1}{r_{ij}}, \tag{6}$$

where c is the speed of light, $\boldsymbol{\alpha}$ and β are the Dirac matrices and V the monopole part of the potential from the extended nuclear charge distribution. The wave function Ψ for a state labeled $\gamma J M_J$, where γ represents the configuration and any other quantum numbers required to specify the state, is approximated by an expansion over jj coupled configuration state functions

$$|\Psi(\gamma J M_J)\rangle = \sum_{j} c_j |\Phi(\gamma_j J M_J)\rangle. \tag{7}$$

The configuration state functions $\Phi(\gamma J)$ are symmetry adapted linear combinations of Slater-determinants built from a set of one-electron relativistic spin-orbitals

$$\phi_{n\kappa m} = \frac{1}{r}\begin{pmatrix} P_{n\kappa}(r)\chi_{\kappa m}(\hat{r}) \\ iQ_{n\kappa}(r)\chi_{-\kappa m}(\hat{r}) \end{pmatrix}. \tag{8}$$

Here κ is the relativistic angular quantum number, $P_{n\kappa}(r)$ and $Q_{n\kappa}(r)$ are the large and small component radial wave functions and $\chi_{\kappa m}(\hat{r})$ is the spinor spherical harmonic in the lsj coupling scheme

$$\chi_{\kappa m}(\hat{r}) = \sum_{m_l,m_s} \langle l\frac{1}{2}m_l m_s \mid jm\rangle Y_{lm_l}(\theta,\varphi)\xi_{m_s}(\sigma). \tag{9}$$

Just as in the non-relativistic case a system of coupled non-linear differential equations for the radial functions can be derived. This system together with the accompanying eigenvalue problem for the expansion coefficients are solved iteratively using the relativistic self-consistent field method [15, 7]. When the set of radial orbitals has been obtained, relativistic configuration interaction (RCI) calculations can be performed. Here the transverse photon interaction as well as the leading QED effects may be included in the Hamiltonian [7].

3. Selection of configuration expansions

In an accurate theoretical study it must be possible to estimate the uncertainty of a given value. Therefore, a whole series of calculations has to be done, where different effects are tested. Notably, it is important to enlarge the CSF expansion in a systematic way in order to ensure convergence of the calculated properties.

An efficient way of choosing the expansion is by the active space method [16, 17]. Here the CSFs of a given symmetry and parity are generated by excitations from one or more important and often closely degenerate reference configurations to an active set of orbitals. The active set of orbitals is then increased in a systematic way, allowing for a monitoring of the convergence of the atomic property being investigated. By imposing restrictions on the way excitations can be done, different correlation effects can be targeted. By allowing all single (S) and double (D) excitations from the reference configurations the energetically dominating pair-correlation effects will be captured [14]. To describe higher order correlation effects triple (T) and quadruple (Q) excitations may also be included.

In order for the configuration expansion not to grow too fast excitations are often done from the outermost shells. For the dominant double excitations we then have a classified according to the following:

(i) if both excitations are from the valence shell the generated CSFs are said to describe outer or valence correlation.

(ii) if there is one excitation from the valence shell and one from a core shell the resulting CSFs describe the polarization of the atomic core and this is referred to as core-valence correlation.

(iii) if both excitations are from the atomic core the generated CSFs are said to describe inner or core-core correlation.

The strategies for choosing the expansions are based on the total energy. For some properties, such as the hyperfine structure, there is a weak coupling with the energy. This means that configurations that may be energetically important are unimportant for the calculated hyperfine structures and vice versa. For hyperfine calculations the expansions described above are often complemented by CSFs obtained by single excitations from deep core shells to account for spin- and orbital polarization [18].

4. Hyperfine structure

The hyperfine structure of the atomic energy levels is caused by the interaction between the electrons and the non-spherical electromagnetic multipole moments of the nucleus. This interaction is known to be very sensitive to electron correlation and relativistic effects, and its study has led to a significant improvement of the understanding of atomic structure.

The hyperfine interaction couples the electronic, J, and nuclear, I, angular momenta to a total momentum $F = I + J$. The eigenfunction of the coupled state is $|\gamma JIFM_F\rangle$ and the leading energy correction to the fine structure level J due to the hyperfine interactions is

$$\Delta E_{hfs} = \frac{1}{2}A_J C + B_J \frac{\frac{3}{4}C(C+1) - I(I+1)J(J+1)}{2I(2I-1)J(2J-1)} \tag{10}$$

where $C = F(F+1) - J(J+1) - I(I+1)$ and

$$A_J = \frac{\mu_I}{I}\frac{1}{[J(J+1)(2J+1)]^{1/2}}\langle \gamma J \| \mathbf{T}^{(1)} \| \gamma J \rangle \tag{11}$$

$$B_J = 2Q\frac{2J(2J-1)}{[(2J+1)(2J+2)(2J+3)]^{1/2}}\langle \gamma J \| \mathbf{T}^{(2)} \| \gamma J \rangle \tag{12}$$

Here $\langle \gamma J \| \mathbf{T}^{(1)} \| \gamma J \rangle$ and $\langle \gamma J \| \mathbf{T}^{(2)} \| \gamma J \rangle$ are reduced matrix elements of one-particle tensor operators. These matrix elements are readily evaluated from the MCHF or MCDHF wave functions (see [10, 11] for details). μ_I and Q are the magnetic dipole and electric quadrupole moments. The magnetic dipole moment is often known with high precision, but the electric quadrupole moment is difficult to determine by direct nuclear techniques. By combining measured B_J values with the computed matrix element $\langle \gamma J \| \mathbf{T}^{(2)} \| \gamma J \rangle$ the nuclear quadrupole moment can be obtained. This method has successfully been used by Sundholm [19, 20, 21] for a large number of isotopes of light atoms. The method has also been extended to heavy relativistic systems [22, 23].

The hyperfine structure in sodium has for many years been a test case for different theoretical methods. In Table 1 calculated A values from large-scale MCHF calculations [24] are compared with values from relativistic many-body perturbation (RMBPT) [25, 26] and coupled-cluster (CCSD) [27] calculations and from experiment. By combining the measured B_J value with the matrix element of the electric quadrupole operator the electric quadrupole moment Q was derived. The MCHF calculations included (SD) excitations from all shells to a large orbital basis. In addition important configurations from (T) excitations were included in the expansion. Although the configurations from the triple excitations are energetically rather unimportant they give a significant contribution to the hfs. The different calculated A values are all in good agreement with experiment. For the quadrupole moment Q the derived atomic values agree very well. There is however a disagreement with the value derived from muonic experiments [35] which led Sundholm and Olsen to doubt the accuracy of the latter [20].

As another application we look at the $6s6p\ ^3P_1$ state in mercury, a complex and relativistic system. Values of the A factor and the electric quadrupole moment Q obtained from MCDHF calculations [36], using the graspVU code, are displayed in Table 2. In the calculations different effects are systematically probed including core-core effects in the outermost core shells. Although the correlation corrections to the Dirac-Fock (DF) values are dominating, QED and the Bohr-Weisskopf effects are also of importance. Figure 1 displays the convergence of the computed parameters as different correlation effects are probed and the number of configurations increase.

Table 1. The interaction constants A_J and electric quadrupole moment Q for $3s\ ^2S_{1/2}$ and $3p\ ^2P_{1/2,3/2}$ states in $^{23}_{11}$Na from MCHF calculations compared with values from other calculations and from experiment (from [24]).

	$3s\ ^2S$	$3p\ ^2P$			
Method	$A_{1/2}$ (MHz)	$A_{1/2}$ (MHz)	$A_{3/2}$ (MHz)	Q (mb)	Reference
HF	626.2	63.66	12.72	171.2	[24]
MCHF+CI	870.3	93.16	18.74	106.1	[24]
MCHF+CI[a]	882.2	94.04	18.80	105.6	[24]
CCSD[a]	883.8	93.02	18.318	104.2	[27]
RMBPT[b]	860.9	91.40	19.80		[25]
RMBPT[c]	884.5				[26]
FE-MCHF[d]				107.1	[20]
Experiment	885.813 064 4(5)	94.42(19)	18.69(6)		[28, 29, 30]
		94.44(13)	18.62(21)		[31]
			18.64(6)		[32]
			18.534(15)		[33]
			18.79(12)		[34]
				100.6(20)	Muonic experiment [35]

[a] Corrected for relativistic effects using the ratio between DF and HF values.
[b] Relativistic many-body perturbation calculation third-order calculation.
[c] Relativistic many-body perturbation calculation all-order calculation.
[d] Corrected for relativistic effects using results from quasirelativistic CI calculations.

Figure 1. The mercury-201 hyperfine magnetic dipole constant A_1 and nuclear quadrupole moment Q as functions of the number of CSFs in the expansion. Note how the values oscillate before the different correlation effects are saturated. For the nuclear quadrupole moment Q values from different experimental methods are indicated at the right. The deduced atomic value $Q = 387$ mb is in agreement with the standard value of Raghavan [37].

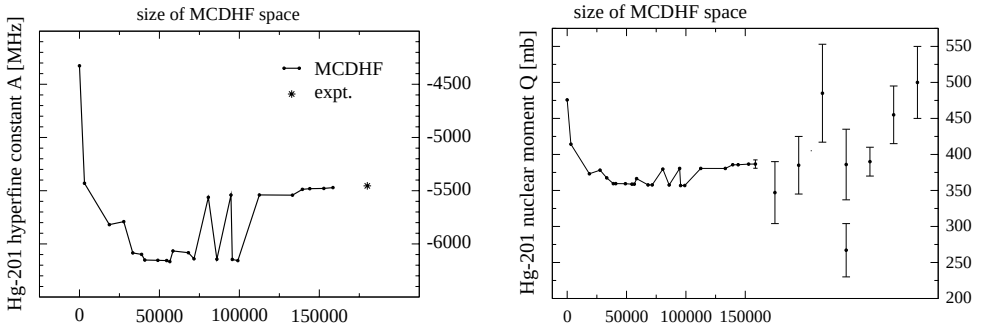

5. Hyperfine induced transitions

The hyperfine interaction, although weak, not only shifts and splits the individual J levels, but also mixes wave functions with different J quantum numbers. This mixing may open new decay channels to different lower levels. To illustrate the effect we look at $nsnp\ ^3P^o_0$. This state is pure in the absence of the hyperfine interaction and can, when the hyperfine interaction is included, be written as

$$|''nsnp\ ^3P^o_0 I(F=I)''\rangle = c_0|nsnp\ ^3P^o_0 I(F=I)\rangle + \sum_i c_i|\gamma_i J_i I(F=I)\rangle =$$

$$c_0|nsnp\ ^3P^o_0 I(F=I)\rangle + c_1|nsnp\ ^3P^o_1 I(F=I)\rangle + c_2|nsnp\ ^1P^o_1 I(F=I)\rangle + \ldots . \qquad (13)$$

Table 2. Calculated values of the magnetic dipole interaction constant A and nuclear electric quadrupole moment Q for the $6s6p\ ^3P_1$ state in $^{201}_{80}$Hg from MCHFD and RCI calculations (from [36]). DF – uncorrelated Dirac-Fock; vv – valence correlation; cv – core-valence; cc – core-core.

Model	A_1 (MHz)	Q (mb)
DF	−4368.266	478.713
vv	−5846.665	389.549
vv + cv	−6216.632	359.056
vv + cv + cc	−5523.861	389.035
Breit and QED	−20.739	-2.409
Bohr-Weisskopf	+73.790	
total	−5470.810	386.626
exp. [38]	−5454.569(0.003)	

The use of quotation marks in the left-hand side term notation highlights the fact that the notation is just a label indicating the dominant character of the eigenvector, which actually is a mixing eigenvectors with different J values. The $nsnp\ ^3P_0^o \rightarrow ns^2\ ^1S_0$ transition now becomes allowed through the finite value of the mixing coefficients $c_1, c_2, \ldots$. Figure 2 depicts the different transitions in the $nsnp\ ^3P_{0,1,2}^o \rightarrow ns^2\ ^1S_0$ multiplet.

Figure 2. Term diagram illustrating the transitions in the $nsnp\ ^3P_{0,1,2}^o \rightarrow ns^2\ ^1S_0$ multiplet. The $J = 2 \rightarrow J' = 0$ transition is dominated by the magnetic quadrupole decay (M2), but with some contributions from the HPF induced mechanism. The $J = 1 \rightarrow J' = 0$ is the intercombination (IC) transition and $J = 0 \rightarrow J' = 0$ is the hyperfine induced transition.

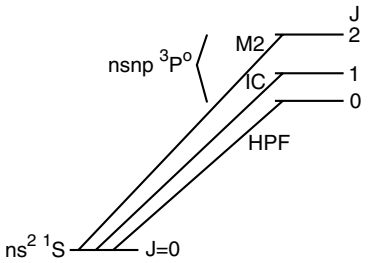

In first-order perturbation theory the mixing coefficients c_i are given by (we consider only the magnetic dipole interaction and states with $J_i = 1$ to simplify things)

$$c_i = \frac{H_{i0}}{E(nsnp\ ^3P_0^o) - E(\gamma_i J_i = 1)} \tag{14}$$

where

$$H_{i0} = \frac{\mu_I}{\sqrt{3}}(1 + 1/I)^{1/2}\langle \gamma_i J_i = 1 \| \mathbf{T}^{(1)} \| nsnp\ ^3P_0^o \rangle \tag{15}$$

is the off-diagonal hyperfine interaction (see [39]). The line strength for the transition is given by

$$S(nsnp\ ^3P_0^o \rightarrow ns^2\ ^1S_o) = \left| \sum_i c_i \langle \gamma_i J_i = 1 \| \mathbf{D}^{(1)} \| ns^2\ ^1S_0 \rangle \right|^2 \tag{16}$$

where the transition matrix element $\langle \gamma_i J_i = 1 \| \mathbf{D}^{(1)} \| ns^2\ ^1S_0 \rangle$ can be evaluated from MCHF or MCDHF wave functions. The line strength is related to the transition rate through the equation

$$A(nsnp\ ^3P^0_o \rightarrow ns^2\ ^1S_0) = \frac{4(2\pi)^2}{9\hbar\lambda^3} S(nsnp\ ^3P^0_o \rightarrow ns^2\ ^1S_0). \quad (17)$$

Calculation of hyperfine induced transitions are difficult in that the generated wave functions need to accurately describe both the off-diagonal hyperfine interaction and the transition matrix elements. Following the pioneer work by Mohr [40] on Helium like ions, efforts have been done using MCHF and MCDHF [41, 39]. In Table 3 calculated rates for the different transitions in the $2s2p\ ^3P^o_{0,1,2} \rightarrow 2s^2\ ^1S_0$ multiplet are shown for selected ions in the Be-sequence. Recently the hyperfine induced transition in N IV was observed in the planetary nebula NGC3918, using the Space Telescope Imaging Spectrograph (STIS) on the Hubble Space Telescope [42]. The calculated rates of the transition for ^{14}N and ^{15}N are in excellent accord with the observational results.

Table 3. Calculated transition probabilities for the Be isoelectronic sequence. For the hyperfine induced transitions (hpf), the transition probabilities are given for the most abundant isotope with $I \neq 0$ (from [39]).

	$^1S_0 - \ ^3P^o_0$	$^1S_0 - \ ^3P^o_1$	$^1S_0 - \ ^3P^o_2$
Ion	HPF	IC	M2
C III	$9.04 \cdot 10^{-4}$	$1.05 \cdot 10^{2}$	$5.14 \cdot 10^{-3}$
N IV	$4.92 \cdot 10^{-4}$	$5.80 \cdot 10^{2}$	$1.14 \cdot 10^{-2}$
O V	$1.52 \cdot 10^{-2}$	$2.28 \cdot 10^{3}$	$2.15 \cdot 10^{-2}$
Ne VII	$6.54 \cdot 10^{-3}$	$1.92 \cdot 10^{4}$	$5.77 \cdot 10^{-2}$
Na VIII	$1.28 \cdot 10^{-1}$		
Mg IX	$2.72 \cdot 10^{-2}$	$9.72 \cdot 10^{4}$	$1.25 \cdot 10^{-1}$
Al X	$8.13 \cdot 10^{-1}$		
Si XI	$6.08 \cdot 10^{-2}$	$3.95 \cdot 10^{5}$	$2.44 \cdot 10^{-1}$
Ca XVII	$1.08 \cdot 10^{0}$		
Fe XXIII	$5.45 \cdot 10^{-2}$	$9.37 \cdot 10^{8}$	$7.95 \cdot 10^{0}$
Ni XXV	$2.46 \cdot 10^{0}$		

6. Summary and conclusion

The development of space-based observatories has lead to a rapid increase in demand from astrophysics for isotope shift, hyperfine structure and and other broadening parameters as well as transition rates. In this article we have tried to indicate how computational atomic physics are responding to this challenge by giving some examples from large scale computations of hyperfine structure parameters and hyperfine quenching. To improve computational methods as well as to understand their limitations, accurate experimental lifetime values for long lived atomic states are of utermost importance.

The ATSP2K–MCHF and graspVU codes used in this research can, along with accompanying documentation, be downloaded from `http://atoms.vuse.vanderbilt.edu/`.

Acknowledgement

PJ gratefully acknowledges support from the Swedish International Development Cooperation Agency (SIDA).

References

[1] R.L. Kurucz, Phys. Scr. **T47**, 110 (1993).
[2] H. Hühnermann, Phys. Scr. **T47**, 70 (1993).
[3] C.R. Proffitt, P. Jönsson, U. Litzén, J.C. Pickering, and G.M. Wahlgren, ApJ, **516**, 342 (1999).
[4] A. Jorissen, Phys. Scr. **T112**, 73 (2004).
[5] E. Träbert, Canadian Journal of Physics **80**, 1481 (2002).
[6] C. Froese-Fischer, G. Tachiev, G. Gaigalas, M. Godefroid, and P. Jönsson, Comput. Phys. Commun. (in preparation) (2005).
[7] F.A. Parpia, C. Froese Fischer, and I.P. Grant, Comput. Phys. Commun. **94**, 249 (1996).
[8] P. Jönsson, X. He, and C. Froese Fischer, unpublished (1998).
[9] J. Olsen, M.R. Godefroid, P. Jönsson, P.Å. Malmqvist, and C. Frose Fischer, Phys. Rev. E **52**, 4499 (1995).
[10] P. Jönsson,C.-G. Wahlström, and C. Froese Fischer, Comput. Phys. Commun. **74**, 399 (1993).
[11] P. Jönsson F.A. Parpia, and C. Froese Fischer, Comput. Phys. Commun. **96**, 301 (1996).
[12] P. Jönsson and C. Froese Fischer, Comput. Phys. Commun. **100**, 81 (1997).
[13] P. Jönsson and S. Gustafsson, Comput. Phys. Commun. **144**, 188 (2002).
[14] C. Froese Fischer, T. Brage, and P. Jönsson, *Computational Atomic Structure; an MCHF approach.* (Institute of Physics Publishing, Bristol and Philadelphia, 1997)
[15] I.P. Grant, Comput. Phys. Commun. **84**, 59 (1994).
[16] B.O. Roos, P.R. Taylor, and P.E.M. Siegbahn, Chem. Phys. **48**, 157 (1980).
[17] J. Olsen, B.O. Roos, P. Jörgensen, and J. Simons, Chem. Phys. Lett. **169**, 463 (1990).
[18] I. Lindgren, Rep. Prog. Phys. **47**, 345 (1984).
[19] D. Sundholm and J. Olsen, J. Phys. Chem. **96**, 627 (1992).
[20] D. Sundholm and J. Olsen, Phys. Rev. Lett. **68**, 927 (1992).
[21] M. Tokman, D. Sundholm, and P. Pyykkö, Chem. Phys. Lett. **291**, 414 (1998).
[22] J. Bieroń and P. Pyykkö, Phys. Rev. Lett. **87**, 133003 (2001).
[23] J. Bieroń and P. Pyykkö, Phys. Rev. A **71**, 032502 (2005).
[24] P. Jönsson, A. Ynnerman, C. Froese Fischer, M.R. Godefroid, and J. Olsen, Phys. Rev. A **53**, 4021 (1996).
[25] W.R. Johnson, M. Idrees, and J. Sapirstein, Phys. Rev. A **35**, 3218 (1987).
[26] Z. Liu, Ph.D. thesis, University of Notre Dame (1989).
[27] S. Salomonson and A. Ynnerman, Phys. Rev. A **43**, 2614 (1990).
[28] A. Beckman, K.D. Böklen, and D. Elke, Z. Phys. **270**, 173 (1974).
[29] J. Carlsson, P. Jönsson, L. Sturesson, and C. Froese Fischer, Phys. Scr. **46**, 394 (1992).
[30] J. Carlsson, Z. Phys. D **9**, 147 (1988).
[31] W.A. Wijngaarden and J. Li, Z. Phys. D **32**, 67 (1994).
[32] Th Krist, P. Kuske, A. Gaupp, W. Wittmann, and H.J. Andrä, Phys. Lett. **A61**, 94 (1977).
[33] W. Yei, A. Sieradzan and M.D. Havey, Phys. Rev. A **48**, 1909 (1993).
[34] U. Volz, M. Majerus, H. Liebel, A. Schmitt, and H. Schmoranzer, Phys. Rev. Lett. **76**, 2862 (1996).
[35] B. Jeckelmann *et al.* Nucl. Phys. A **408**, 495 (1983).
[36] J. Bieroń, P. Pyykkö, and P. Jönsson, Phys. Rev. A **71**, 012502 (2005).
[37] P. Raghavan, At. Data Nucl. Data Tables **42**, 189 (1989).
[38] R.H. Kohler, Phys. Rev. **121**, 1104 (1961).
[39] T. Brage, P.G. Judge, A. Aboussaïd, M.R. Godefroid, P. Jönsson, A. Ynnerman, C. Froese Fischer, and D.S. Leckrone, ApJ. **500**, 507 (1998).
[40] P. Mohr, in *Beam-Foil Spectroscopy, Atomic Structure and Lifetimes*, edited by I. Sellin and D. Pegg (Plenum, New York, 1976), Vol. 1, pp. 97-103.
[41] A. Aboussaïd, M.R. Godefroid, P. Jönsson, and C. Froese Fischer, Phys. Rev. A **51**, 2031 (1995).
[42] T. Brage, P.G. Judge, and C. Proffitt, Phys. Rev. Lett. **89**, 281101-1 (2002).